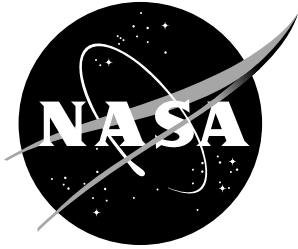


NASA/TM-2003-211755  
ARL-TR-2774



# Analytical and Experimental Study of Near-Threshold Interactions Between Crack Closure Mechanisms

*John A. Newman*  
*U.S. Army Research Laboratory*  
*Vehicle Technology Directorate*  
*Langley Research Center, Hampton, Virginia*

*William T. Riddell*  
*U.S. Department of Transportation*  
*Volpe National Transportation Systems Center*  
*Cambridge, Massachusetts*

*Robert S. Piascik*  
*Langley Research Center, Hampton, Virginia*

## The NASA STI Program Office ... in Profile

Since its founding, NASA has been dedicated to the advancement of aeronautics and space science. The NASA Scientific and Technical Information (STI) Program Office plays a key part in helping NASA maintain this important role.

The NASA STI Program Office is operated by Langley Research Center, the lead center for NASA's scientific and technical information. The NASA STI Program Office provides access to the NASA STI Database, the largest collection of aeronautical and space science STI in the world. The Program Office is also NASA's institutional mechanism for disseminating the results of its research and development activities. These results are published by NASA in the NASA STI Report Series, which includes the following report types:

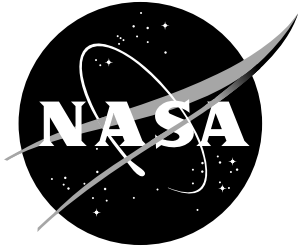
- TECHNICAL PUBLICATION. Reports of completed research or a major significant phase of research that present the results of NASA programs and include extensive data or theoretical analysis. Includes compilations of significant scientific and technical data and information deemed to be of continuing reference value. NASA counterpart of peer-reviewed formal professional papers, but having less stringent limitations on manuscript length and extent of graphic presentations.
- TECHNICAL MEMORANDUM. Scientific and technical findings that are preliminary or of specialized interest, e.g., quick release reports, working papers, and bibliographies that contain minimal annotation. Does not contain extensive analysis.
- CONTRACTOR REPORT. Scientific and technical findings by NASA-sponsored contractors and grantees.
- CONFERENCE PUBLICATION. Collected papers from scientific and technical conferences, symposia, seminars, or other meetings sponsored or co-sponsored by NASA.
- SPECIAL PUBLICATION. Scientific, technical, or historical information from NASA programs, projects, and missions, often concerned with subjects having substantial public interest.
- TECHNICAL TRANSLATION. English-language translations of foreign scientific and technical material pertinent to NASA's mission.

Specialized services that complement the STI Program Office's diverse offerings include creating custom thesauri, building customized databases, organizing and publishing research results ... even providing videos.

For more information about the NASA STI Program Office, see the following:

- Access the NASA STI Program Home Page at <http://www.sti.nasa.gov>
- E-mail your question via the Internet to [help@sti.nasa.gov](mailto:help@sti.nasa.gov)
- Fax your question to the NASA STI Help Desk at (301) 621-0134
- Phone the NASA STI Help Desk at (301) 621-0390
- Write to:  
NASA STI Help Desk  
NASA Center for AeroSpace Information  
7121 Standard Drive  
Hanover, MD 21076-1320

NASA/TM-2003-211755  
ARL-TR-2774



# Analytical and Experimental Study of Near-Threshold Interactions Between Crack Closure Mechanisms

*John A. Newman*  
*U.S. Army Research Laboratory*  
*Vehicle Technology Directorate*  
*Langley Research Center, Hampton, Virginia*

*William T. Riddell*  
*U.S. Department of Transportation*  
*Volpe National Transportation Systems Center*  
*Cambridge, Massachusetts*

*Robert S. Piascik*  
*Langley Research Center, Hampton, Virginia*

National Aeronautics and  
Space Administration

Langley Research Center  
Hampton, Virginia 23681-2199

---

May 2003

---

Available from:

NASA Center for AeroSpace Information (CASI)  
7121 Standard Drive  
Hanover, MD 21076-1320  
(301) 621-0390

National Technical Information Service (NTIS)  
5285 Port Royal Road  
Springfield, VA 22161-2171  
(703) 605-6000

## Abstract

*The results of an analytical closure model that considers contributions and interactions between plasticity-, roughness-, and oxide-induced crack closure mechanisms are presented and compared with experimental data. The analytical model is shown to provide a good description of the combined influences of crack roughness, oxide debris, and plasticity in the near-threshold regime. Furthermore, analytical results indicate that closure mechanisms interact in a non-linear manner such that the total amount of closure is not the sum of closure contributions for each mechanism.*

## Introduction

Fatigue crack closure occurs when crack faces contact during cyclic loading. According to Elber's model (ref. 1), fatigue damage only occurs during the portion of the load cycle where the crack faces are open. Cracks are expected to be closed for greater portions of the load cycle at low load ratio ( $R = K_{\min}/K_{\max}$ , where  $K_{\min}$  and  $K_{\max}$  are the minimum and maximum values of the crack-tip stress intensity factor, respectively) so crack closure has been used to explain R-effects on fatigue crack growth (FCG) rates, *i.e.*, increases in crack growth rate occur with increases in  $R$ . A crack closure model was developed that considers plasticity-, roughness-, and oxide-induced crack closure mechanisms (PICC, RICC, and OICC, respectively); the closure mechanisms most likely to occur at FCG threshold (refs. 2 and 3). This model, named the CROP model (for Closure, Roughness, Oxide, and Plasticity), is believed to be uniquely suited for threshold FCG scenarios because no existing closure models include contributions and interactions of all three of these closure mechanisms

## Objectives

The objectives of this paper are to (1) validate the CROP model with experimental data, (2) discuss the implications of the CROP model results, and (3) examine interactions between PICC, RICC, and OICC. Once shown in good agreement with experimental data, the model will be used to examine interactions between closure mechanisms. Several models exist that consider only a single closure mechanism (refs. 4-7), but it is not clear how to determine the effects of multiple closure mechanisms from analytical results that consider individual mechanisms. The simplest way to combine single-mechanism model results is a linear superposition, shown in Equation 1. However, analytical and experimental results presented later in this paper show a simple linear superposition is not sufficient to predict closure behavior and interactions of multiple mechanisms.

$$R_{cl} = R_{cl}|_{PICC} + R_{cl}|_{RICC} + R_{cl}|_{OICC} \quad (1)$$

## Model Description

The CROP model idealizes rough cracks as two-dimensional sawtooths, shown schematically in Figure 1. This crack configuration is described by two parameters: an asperity angle,  $\alpha$ , and an asperity length,  $g$ . Crack-tip displacements are calculated in terms of applied loads and crack geometry. Due to the rough crack geometry, mixed-mode crack-face displacements occur, even when far-field loading conditions are strictly mode I (ref. 8). Similar to other closure models (refs. 4, 5, and 8-13), crack-face displacements are used to compute crack closure loads. However, the CROP model is unique because it

considers three closure mechanisms and distinguishes between crack-wake contact at two different locations due to roughness effects. Single-mechanism models are limited because different closure mechanisms are likely to dominate in the Paris and threshold FCG regimes, possibly contacting at different crack-wake locations. The CROP model should work well for both the Paris regime and near-threshold FCG because PICC, RICC, and OICC (the closure mechanisms considered most important at the FCG threshold) are considered.

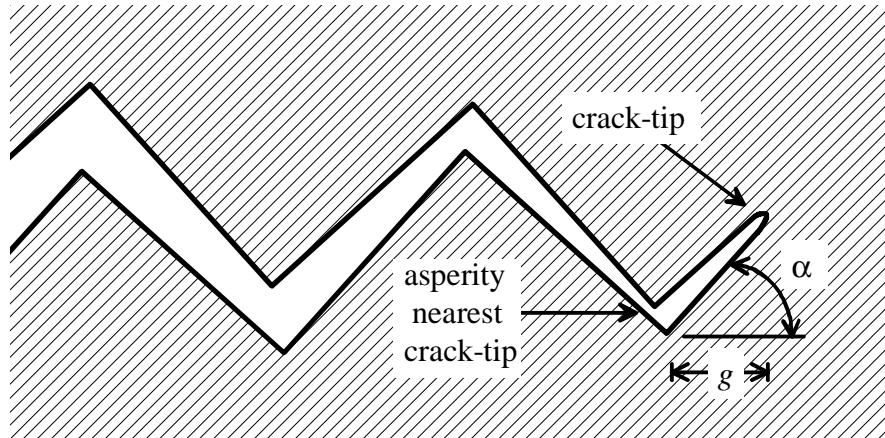


Figure 1. Schematic of the idealized rough crack geometry used by the CROP model. This crack configuration is described by two parameters: asperity angle,  $\alpha$ , and asperity length,  $g$ .

Analysis of straight cracks, where crack-wake roughness is not a factor, indicates that closure first occurs at the crack tip (*i.e.* called “tip contact”) (ref. 14). However, analysis of rough cracks shows that closure might occur first at the asperity nearest the crack-tip (*i.e.* called “asperity contact”) (refs. 2 and 3). Depending on geometry and loading conditions, it is possible for closure to occur first at either location. Therefore, the CROP model considers both tip contact and asperity contact. These locations are very close (within 100  $\mu\text{m}$  for most alloys), and contact at either location can completely shield the crack-tip from further damage.\* For simplicity, only the first closure event (during unloading) is considered to be important, so the CROP model computes closure levels at both locations, but only uses the greater value. For example, if asperity contact is predicted at  $R_{cl} = 0.5$  and tip contact at  $R_{cl} = 0.3$ , then asperity contact dominates, and tip contact results are neglected.†

## Test Procedures

A series of experiments was performed using two aluminum alloys (2024 and 8009) to evaluate analytical model results. The quality of the agreement between analytical results and experimental data will determine the validity of the CROP model, at least for aluminum alloys. Analytical results are also compared with data found in the literature for aluminum (ref. 18), steel (refs. 19 and 20), and nickel-based alloys (ref. 21).

FCG tests were performed by cyclically loading laboratory specimens in closed-loop servo-hydraulic testing machines. An automated computer-controlled system continuously monitored crack length during

\* Closure may occur behind the crack-tip due to load-history effects that only partially shield the crack tip from damage after contact (refs. 15-17). Partial crack closure is not considered here.

† Results are presented in terms of the load ratio at closure,  $R_{cl} = K_{cl}/K_{max}$ , called closure level, where  $K_{cl}$  is the value of the crack-tip stress intensity factor where crack closure occurs.

tests from back-face strain data (ref. 22) and adjusted loads to achieve programmed stress-intensity factors. This system allows FCG tests to be performed in K-control, *i.e.* controlling stress intensity factors while testing. As summarized in Table 1, data from the literature was obtained with compact-tension (CT) specimens (ref. 23), while the authors used eccentrically-loaded-single-edge-notch tension (ESET) specimens (ref. 24).<sup>‡</sup>

Table 1. Details of FCG specimen configuration and geometry.

Alloy	specimen configuration	specimen width (mm)	specimen thickness (mm)
2024 aluminum (L-T)	ESET	38.1	2.28
8009 aluminum (L-T)	ESET	38.1	2.28
<i>Data from literature</i>			
8009 aluminum (T-L) <sup>1</sup>	CT	57.2	6.35
AISI 1080 steel (CG) <sup>2</sup>	CT	63.5	6.35
AISI 1080 steel (FG) <sup>2</sup>	CT	63.5	6.35
Grade E drill pipe steel <sup>3</sup>	CT	63.0	6.30
INCONEL 718 (CG) <sup>4</sup>	CT	38.0	3.80
INCONEL 718 (FG) <sup>4</sup>	CT	38.0	3.80

<sup>1</sup> From McEvily (ref. 18)

<sup>2</sup> From Gray, *et al.* (ref. 19)

<sup>3</sup> From Ruppen, *et al.* (ref. 20)

<sup>4</sup> From Drury, *et al.* (ref. 21)

## Closure determination

Changes in compliance that occur when fatigue cracks close are used to determine crack closure loads (ref. 25). Closure determinations were made here with compliance data measured near the crack tip and at the specimen back face. Typically, closure determinations are made with far-field (*i.e.* measured far from the crack-tip) compliance data at the crack mouth or specimen back-face. Back-face strain closure determinations were used, and are attractive because they are easily obtained and require no additional equipment. (Recall that back-face strain is already used to monitor crack length.) However, this technique provides only a “global” closure value with no information about contact location, *i.e.* whether tip contact or asperity contact occurs. Also, global closure determinations are thought to lack the sensitivity needed to resolve near-tip closure events at threshold (ref. 26). Therefore, an alternative non-contacting near-tip technique called DIDS (Digital Image Displacement System) was used. Crack-tip deformations are obtained by analyzing a series of high magnification digital images of the crack-tip region during fatigue loading (refs. 27 and 28). As with global determinations, DIDS uses compliance changes to measure closure loads. DIDS provides “local” closure values more sensitive to near-tip closure events because near-crack-tip deformations are used. Unlike global determinations, local closure determinations can be made at any location along the crack, providing closure data at specific points.

<sup>‡</sup> The ESET specimen was formerly called extended-compact-tension (ECT) specimen (ref. 24).

DIDS can even detect differences between tip contact and asperity contact at threshold (refs. 3 and 29). Herein, closure determinations using far-field and near-tip compliance data are called global and local, respectively.

### Model verification strategy

To understand the complex interactions between plasticity-, roughness-, and oxide-induced crack closure (PICC, RICC, and OICC, respectively), an experimental plan was developed to isolate and quantify the influence of each closure mechanism. This was accomplished by performing a series of experiments with carefully selected combinations of alloy and environment that produce the required crack-tip closure attributes. By selecting a specific alloy and environment, individual closure mechanisms can be enhanced (turned on) or eliminated (turned off), as shown in Table 2.

**RICC** – Aluminum alloy 8009 was selected because the powder metallurgy (PM) alloy has an extremely fine-grain (FG) size that results in an extremely flat fatigue crack surface such that RICC effects are negligible (refs. 3 and 30). The effects of plasticity and oxide can be studied in the absence of RICC by testing 8009 aluminum specimens. Aluminum alloy 2024 has a course microstructure that results in rough fatigue crack surfaces (in comparison to alloy 8009) and will be used to study crack roughness effects. RICC can be turned on or off by selecting aluminum alloy 2024 or 8009, respectively.

**OICC** – FCG tests were performed in ultra-high vacuum (UHV) to eliminate crack mouth oxide and allow PICC and RICC to be studied without OICC.<sup>§</sup> Crack mouth oxide layers produced in laboratory air environments are typically thin (about 10-100 Å thick for aluminum alloys, refs. 6 and 31) and will later be shown to have a negligible closure contribution. Rather than perform FCG tests in corrosive environments and measure oxide thickness after testing, an artificial oxide layer was created with an alumina (Al<sub>2</sub>O<sub>3</sub>) powder solution injected into the crack mouth. Alumina powder, normally used to polish metal surfaces, is available in large quantities of carefully measured and uniform particle sizes. By using alumina powder, the effective oxide thickness is known during testing and can be changed by using different particle sizes.

**PICC** – Crack-tip plastic deformations remain in the wake of propagating fatigue cracks, resulting in PICC. Elimination of PICC requires the ability to recover (turn off) crack-wake plasticity on command. Although recovery of crack-wake plasticity has been accomplished with a nickel-titanium (Ni-Ti) shape memory alloy (refs. 3 and 29), these results are not discussed here. Instead, the simplest case studied will have only PICC as a closure mechanism (without RICC and OICC).

Table 2. Conditions used to control individual closure mechanisms.

mechanism	ON	OFF
RICC	CG alloy ( <i>e.g.</i> alloy 2024)	FG alloy ( <i>e.g.</i> alloy 8009)
OICC	inject particles into crack	UHV
PICC	normal FCG	shape memory alloy <sup>*</sup>

<sup>\*</sup> See ref. 3

<sup>§</sup> In this paper, UHV indicates pressure less than  $3 \times 10^{-6}$  Pa.

## Experimental Results

Analytical results are compared with experimental data in this section. In each case, the model parameters listed in Table 3 were used to tailor analytical results for specific materials and test conditions. Individual closure mechanisms are activated as needed (see Table 2), allowing consideration of increasingly complex closure scenarios, *i.e.* simple cases considered first.

Table 3. Model parameters used for different alloys.

Alloy	E (GPa)	$\sigma_o$ (MPa)	$\nu$	$g$ ( $\mu\text{m}$ )	$\alpha$ (degrees)
2024 aluminum	72	350	0.3	10	30
8009 aluminum <sup>1</sup>	88	420	0.3	0	0
AISI 1080 steel (CG) <sup>2</sup>	210	410	0.3	74	45
AISI 1080 steel (FG) <sup>2</sup>	210	410	0.3	40.5	45
Grade E Pipe Steel <sup>3</sup>	210	700	0.3	0	0
INCONEL 718 (CG) <sup>4</sup>	200	1410	0.3	9	30
INCONEL 718 (FG) <sup>4</sup>	200	1240	0.3	4	30

<sup>1</sup> Used for data from McEvily (T-L orientation) (ref. 18) and data by authors (L-T orientation).

<sup>2</sup> Used for data from Gray, *et al* (ref.(19)).

<sup>3</sup> Used for data from Ruppen, *et al* (ref. 20).

<sup>4</sup> Used for data from Drury, *et al* (ref. 21).

### Closure due to plasticity (PICC)

As a simple case, consider a straight crack without crack-mouth oxide (*i.e.* no RICC or OICC) where PICC is the only closure mechanism. Model predictions are obtained for this case by setting  $\alpha = 0$  and  $t = 0$ . For comparison, experimental results for 8009 aluminum specimens (no RICC) tested in UHV (no OICC) are used. Only tip contact occurs here in the absence of crack-wake roughness.

The relationship between closure levels ( $R_{cl} = K_{cl}/K_{max}$ ), load ratio ( $R = K_{min}/K_{max}$ ), and  $K_{max}$  are plotted in Figure 2. Analytical results are shown as solid curves and experimental data are indicated by symbols.  $R_{cl}$  is plotted against  $R$  in Figure 2a. The diagonal dotted line corresponds to  $R_{cl} = R$ , *i.e.* closure occurring at minimum load. No closure is predicted for  $R > 0.34$  (where solid and dotted curves intersect) because the solid curve is below the dotted line. Global closure determinations for 8009 aluminum at  $\Delta K = 6.6 \text{ MPa}\sqrt{\text{m}}$  are shown as triangular symbols in Figure 2a; no closure was detected for  $R > 0.30$ . As seen in the figure, the data are in good agreement with analytical results. For this crack configuration, the analytical relation between  $R_{cl}$  and  $R$  is independent of  $K_{max}$ ,  $E$ , and  $\sigma_o$ . Although analytical results in Figure 2a were calculated using parameters for 8009 aluminum (see Table 3), identical results are obtained with any parameters if  $\alpha = 0$  (smooth cracks) and  $t = 0$  (no crack mouth oxide). In other words, closure levels depend only on  $R$  where PICC is the only closure mechanism. <sup>\*\*</sup>

<sup>\*\*</sup> Experimental evidence indicates  $R_{cl}$  increases during constant- $R$  decreasing- $\Delta K$  tests, especially near FCG threshold where RICC, OICC and load-history effects are most significant (refs. 4, 16, 17, and 19-21).

In Figure 2b,  $R_{cl}$  is plotted against  $K_{max}$  for 8009 aluminum loaded at  $R = 0.05$ . The model predicts constant closure levels of  $R_{cl} = 0.25$  for all  $K_{max}$ , shown as the horizontal solid line. Data generated in UHV and laboratory air environments are shown as solid and open symbols, respectively. Triangular and circular symbols indicate global and local closure determinations, respectively. Little difference is observed between closure levels in air and UHV, suggesting that the naturally forming oxide layer in air has a negligible closure contribution, at least for alloy 8009. Published results by McEvily on 8009 aluminum specimens (also tested in air at  $R = 0.05$ , but for the T-L orientation) are shown as cross symbols (ref. 18). All data in Figure 2b are in good agreement with analytical predictions. Based on the data in Figure 2, the CROP model works well where PICC is the only closure mechanism.

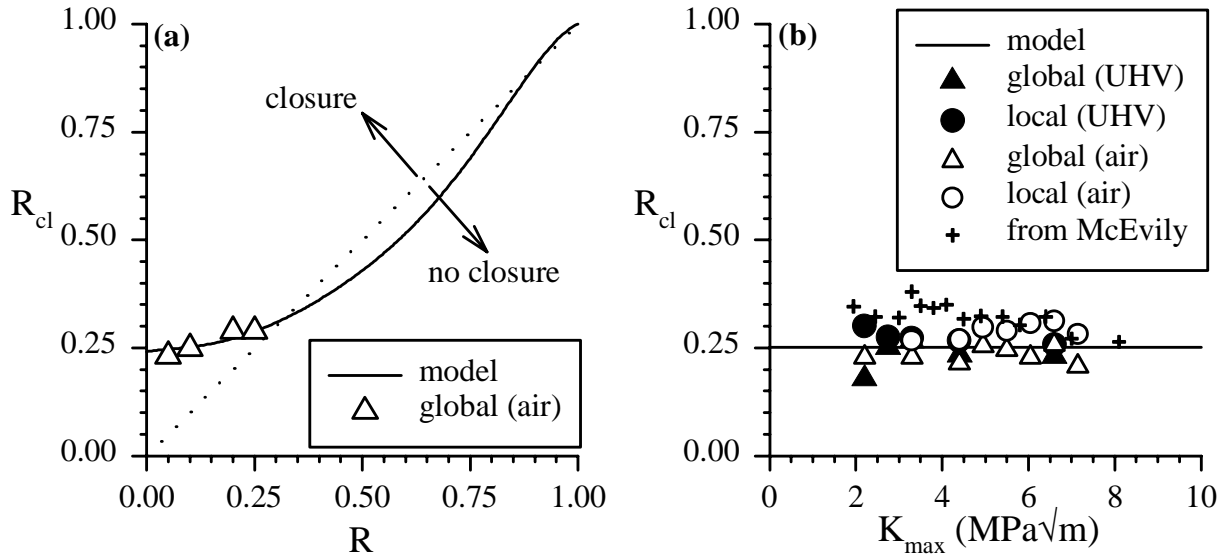


Figure 2. Comparison of model results (solid curve) and experimental data (symbols) where PICC is the only closure mechanism; Here, aluminum alloy 8009 FCG data ( $R = 0.05$ ) are used because the flat featureless crack surface produces little or no RICC. Closure levels are plotted against  $R$  in part (a) and  $K_{max}$  in part (b).

### Closure due to plasticity and oxide (PICC and OICC)

Next, the combination of PICC and OICC is considered. Analytical results for 8009 aluminum at  $R = 0.05$  are shown in Figure 3. In Figure 3a,  $R_{cl}$  is plotted against  $K_{max}$  for oxide layers of 0, 100 and 500 Å thick (solid, dotted, and dashed curves, respectively). As shown in Figure 2b, closure levels are constant for no oxide layer ( $t = 0$ , solid curve). For oxide layers of finite thickness,  $R_{cl}$  increases as  $K_{max}$  decreases because the crack-tip opening displacement (CTOD) becomes smaller in comparison to  $t$ . When  $R_{cl}$  increases to unity ( $R_{cl} = 1$ ) the crack becomes fully closed ( $K_{cl} = K_{max}$ ); this is labeled  $K_{max fc}$  for the  $t = 100$  Å curve. As the oxide thickness increases both  $R_{cl}$  and  $K_{max fc}$  increase. The relation between  $K_{max fc}$  and oxide thickness,  $t$ , is plotted in Figure 3b (solid curve); here,  $K_{max fc}$  is proportional to  $\sqrt{t}$ . Fully closed crack conditions exist in the shaded region below the curve (*i.e.*  $K_{max} < K_{max fc}$ ).

As shown in Figure 2b, the contribution of oxide layers produced in air (typically, on the order of 10-100 Å, refs. 6 and 31) was not detected by local or global closure determinations. Therefore, alumina ( $Al_2O_3$ ) particles were injected into the crack mouth to simulate an artificially thick oxide layer, typical of either aggressive environments or crack surface fretting. As before, tests were performed at  $R = 0.05$ , and 8009 aluminum specimens were used to eliminate RICC. Closure levels are plotted against  $K_{max}$  in Figure 4 for  $Al_2O_3$  particle diameters of (a) 0.05 μm (500 Å) and (b) 0.30 μm (3000 Å). Analytical

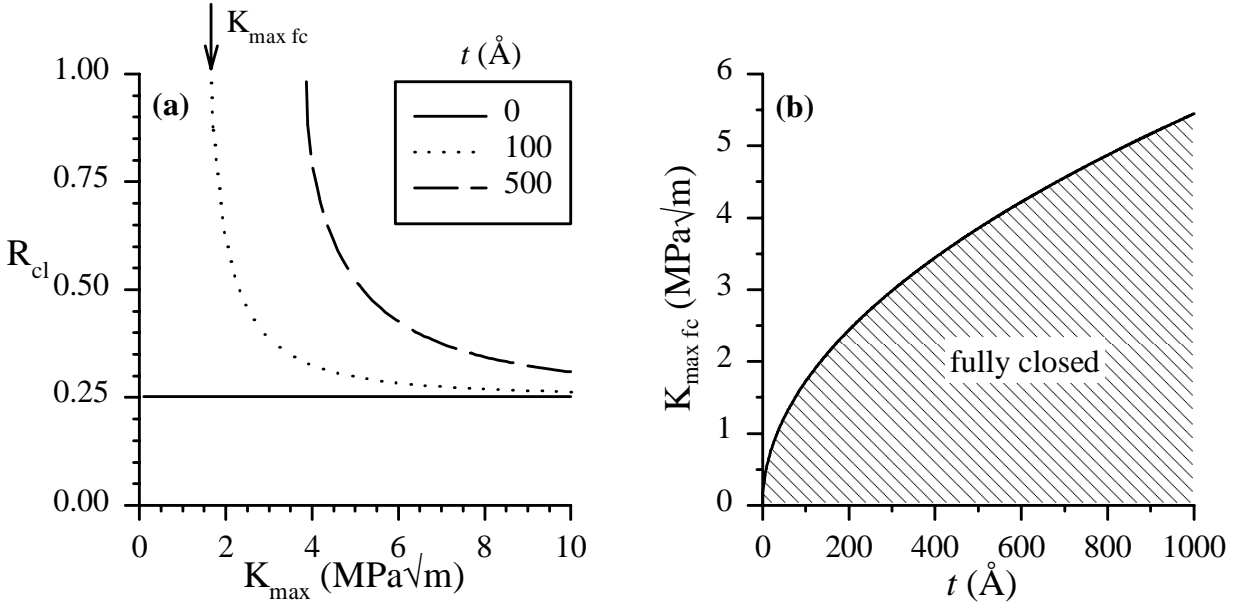


Figure 3. Model results for straight cracks with an oxide layer for aluminum alloy 8009 at  $R = 0.05$ . Closure levels,  $R_{cl}$ , are plotted against  $K_{max}$  for three different values of oxide layer thickness in part (a). The fully closed  $K_{max}$  value,  $K_{max\ fc}$ , is plotted against oxide thickness,  $t$ , in part (b). Fully closed crack conditions occur in the shaded region.

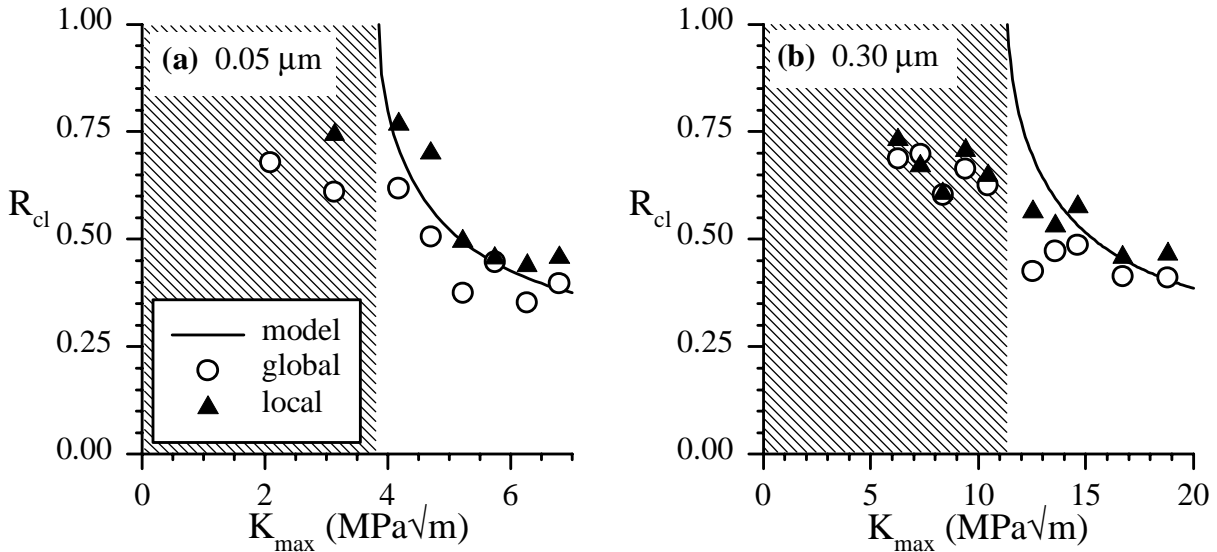


Figure 4. Comparison of model results (solid curve) and experimental data (symbols) where PICC and OICC are closure mechanisms. Aluminum alloy 8009 specimens were used to eliminate roughness, and alumina particles (a) 0.05 μm and (b) 0.30 μm in diameter were injected into the crack mouth to simulate a thick oxide layer. Fully closed conditions are predicted in shaded regions on the left side of the plots.

results are shown by solid curves, and global and local closure determinations are shown as open circular and solid triangular symbols, respectively. The shaded regions on the left sides of the plots correspond to fully closed conditions (*i.e.*  $CTOD_{max} < t$ ). Model results are in good agreement with both global and local data for both particle sizes. Where fully closed crack conditions were predicted (shaded region), analytical results and data diverged because alumina particles were unable to reach the crack tip. (See ref.

3 for details about particles reaching the crack tip.) Therefore, the model predictions (made assuming a uniform oxide layer up to the crack-tip) did not match actual crack-tip conditions. Based on the data in Figure 4, the CROP model accurately predicts the crack closure behavior of cracks subject to both PICC and OICC.

### Closure due to roughness (RICC)

Analytical results for rough cracks are plotted in Figure 5 as  $R_{cl}$  against asperity angle,  $\alpha$ , using parameters for 2024 aluminum (refer to Table 3),  $R = 0.05$ , and  $t = 100 \text{ \AA}$ . Results for  $K_{max}$  values of 2, 4, and 6  $\text{MPa}\sqrt{\text{m}}$  are shown as solid, dotted, and dashed curves, respectively. At low values of  $\alpha$ , tip contact is predicted (near-horizontal region of left side of Figure 5). As  $\alpha$  increases,  $R_{cl}$  gradually increases until asperity contact occurs (near-vertical region on right side of Figure 5). For the  $K_{max} = 2 \text{ MPa}\sqrt{\text{m}}$  curve, the transition between tip contact and asperity contact is labeled as  $\alpha_{trans}$ . Further increases in  $\alpha$  produce rapid increases in  $R_{cl}$  until the crack becomes fully closed, indicated by  $\alpha_{fc}$ . Similar behavior is seen for other  $K_{max}$  levels, although specific values of  $\alpha_{trans}$  and  $\alpha_{fc}$  vary with  $K_{max}$ .

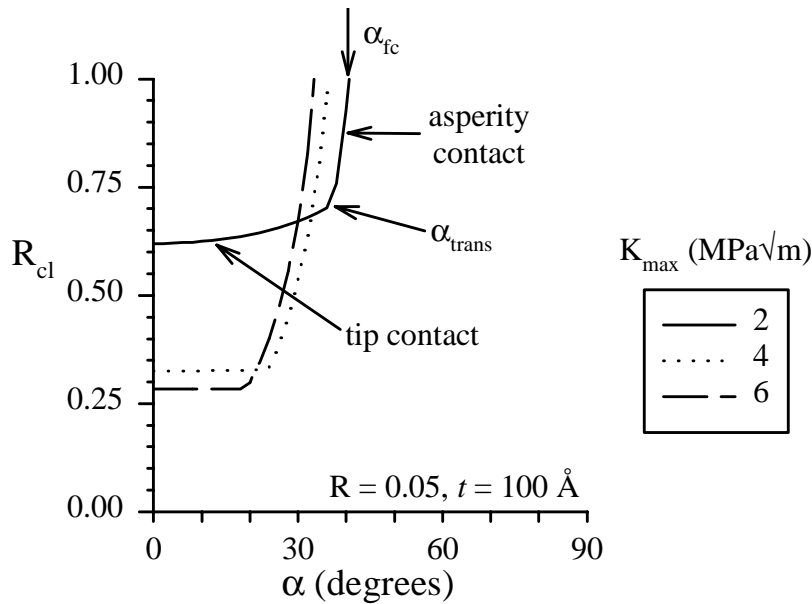


Figure 5. Model results for rough cracks with a  $100 \text{ \AA}$  oxide layer. Closure levels,  $R_{cl}$ , are plotted against  $\alpha$  for three different values of  $K_{max}$ . At small values of  $\alpha$ , tip contact occurs. As  $\alpha$  increases, closure levels gradually increase until a transition to asperity contact occurs at  $\alpha_{trans}$ . Closure levels increase rapidly with further increase in  $\alpha$  until the crack becomes fully closed at  $\alpha_{fc}$ .

The relationships between  $\alpha_{trans}$ ,  $\alpha_{fc}$ , and  $K_{max}$  are shown in Figure 6 for a crack-tip oxide thickness of (a)  $t = 0$  and (b)  $t = 250 \text{ \AA}$  (using parameters for 2024 aluminum and  $R = 0.05$ ). Two solid curves are shown on each plot of  $\alpha$  against  $K_{max}$ ; the upper curve corresponds to  $\alpha_{fc}$  and the lower to  $\alpha_{trans}$ . In both plots, conditions above the upper curve correspond to fully closed cracks and tip contact occurs below the lower curve. Between these curves asperity contact is predicted. For no oxide layer (Figure 6a) these curves intersect at  $\alpha = 60^\circ$  and  $K_{max} = 0$ . This implies cracks will be completely closed if  $\alpha > 60^\circ$ , *i.e.* no FCG occurs. For oxide layers with finite thickness, these curves intersect at positive values of  $K_{max}$ , labeled by  $K_{max \text{ trans}}$  in Figure 6b. Increases in  $t$  are accompanied by increases in  $K_{max \text{ trans}}$ . Tip contact occurs first for any value of  $\alpha$  if  $K_{max \text{ trans}} > K_{max}$ . This implies that crack roughness effects are reduced (because asperity contact becomes less likely) as crack mouth oxide increases. The relationship between

$K_{\max \text{ trans}}$  and  $t$ , for  $R = 0.05$ , is plotted in Figure 7 as a solid curve. Asperity contact (RICC) is not possible for conditions in the shaded region below the curve. Outside the shaded region asperity contact is possible, depending on the asperity angle,  $\alpha$ .

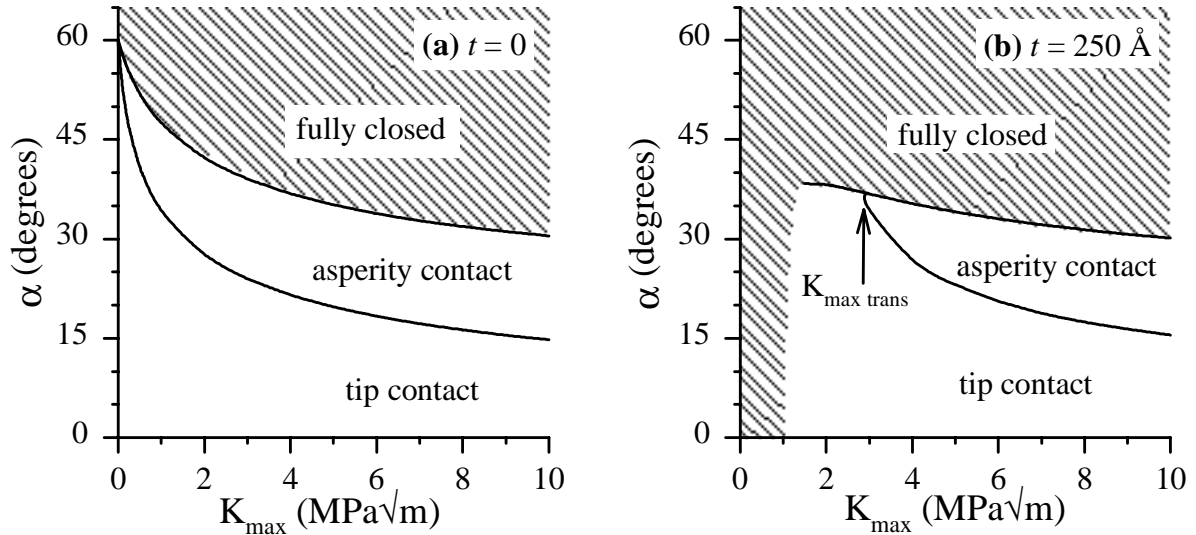


Figure 6. Plots of  $\alpha_{\text{trans}}$  and  $\alpha_{\text{fc}}$  as functions of  $K_{\max}$  for (a) no oxide and (b) a 250  $\text{\AA}$  oxide layer. These curves partition the plots into three regions of crack closure behavior: tip contact, asperity contact, and fully closed crack conditions. These curves intersect at  $K_{\max \text{ trans}}$ , as shown in part (b). No asperity contact occurs for  $K_{\max} < K_{\max \text{ trans}}$ , and  $K_{\max \text{ trans}}$  increases with increasing oxide thickness.

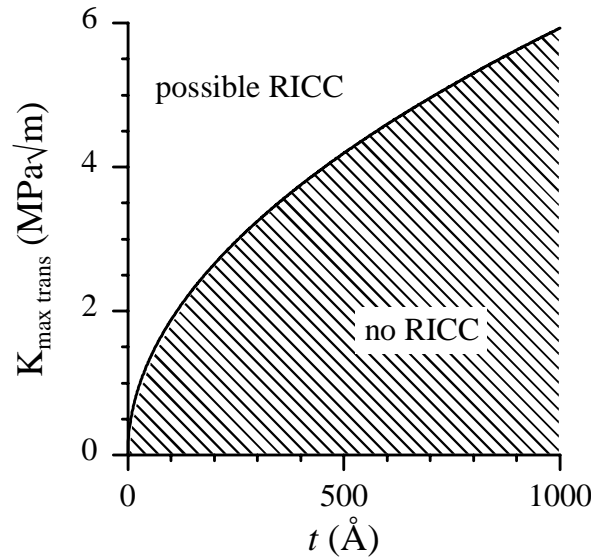


Figure 7. Plot of  $K_{\max \text{ trans}}$  against oxide thickness,  $t$ , for  $R = 0.05$ . Model results indicate asperity contact (*i.e.* RICC) is not possible for conditions below this curve.

Closure data for 2024 aluminum tested at  $R = 0.1$  is compared with analytical results in Figure 8 to examine the validity of the CROP model results. Global and local data, plotted as  $R_{\text{cl}}$  against  $K_{\max}$ , are shown as closed circular and open triangular symbols, respectively. Analytical results are shown as the solid curve. FCG tests were conducted in laboratory air, so a 10  $\text{\AA}$  thick oxide layer was assumed to exist on the crack surfaces (refs. 6 and 31). Analytical results indicate a transition from tip contact to asperity

contact occurs as  $K_{\max}$  decreases to  $3.5 \text{ MPa}\sqrt{\text{m}}$ ; that is, tip contact occurs for  $K_{\max} > 3.5 \text{ MPa}\sqrt{\text{m}}$  and asperity contact for  $K_{\max} < 3.5 \text{ MPa}\sqrt{\text{m}}$ . Closure levels were nearly constant before the transition ( $R_{\text{cl}} \approx 0.25$ ), but  $R_{\text{cl}}$  rapidly increases as  $K_{\max}$  decreases below  $3.5 \text{ MPa}\sqrt{\text{m}}$ , until fully closed conditions occur at  $K_{\max} = 2.9 \text{ MPa}\sqrt{\text{m}}$ . As seen in Figure 8, analytical results are in good agreement with data over the entire range of  $K_{\max}$  presented, including the transition from tip contact to asperity contact.<sup>††</sup>

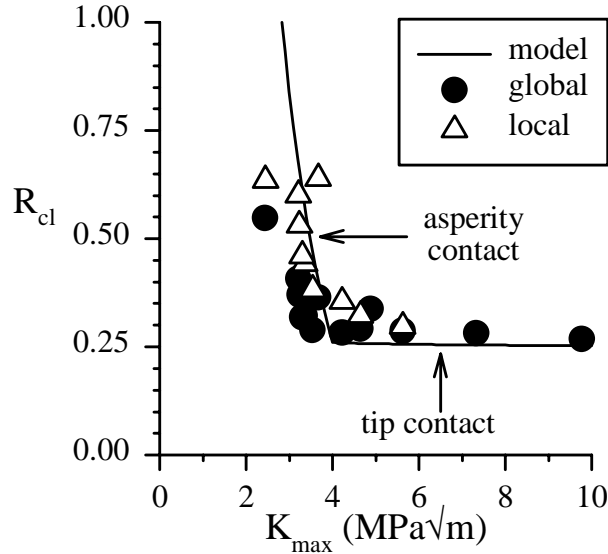


Figure 8. Comparison of model results (solid line) and experimental data (symbols) for 2024 aluminum tested at  $R = 0.1$  in air.

### Comparison with data from literature

Closure measurements on Grade E pipe steel tested in a  $\text{H}_2\text{S}$  brine solution were published by Ruppen, *et al.* (ref. 20). FCG tests were performed at  $R = 0.1$  and 4 Hz for both increasing and decreasing  $K_{\max}$ . The brine solution is corrosive and expected to produce thick crack mouth oxide layers; thicker oxide layers were reported for increasing  $K_{\max}$  conditions (compared with decreasing  $K_{\max}$  conditions), as thick as  $1000 \text{ \AA}$ . The oxide layer thickness in the crack mouth is likely less than surface measurements, but no specific value was reported. (It was shown in Figure 6 that asperity contact is less likely in the presence of thick crack-tip oxide layers, so RICC effects are neglected here, and analytical results were obtained for  $\alpha = 0$  and  $g = 0$ ). Experimentally measured closure levels, plotted against  $K_{\max}$  in Figure 9, for increasing and decreasing  $K_{\max}$  are shown as open circular and closed triangular symbols, respectively. Analytical results for this steel are plotted in the figure for  $t = 0, 250, 500,$  and  $1000 \text{ \AA}$  (dotted, dashed, solid, and dashed-dotted lines, respectively). Data is bounded by analytical results for  $t = 250 \text{ \AA}$  and  $t = 1000 \text{ \AA}$ . Fully closed values for decreasing and increasing  $K_{\max}$  occur at  $K_{\max} = 7.7$  and  $10.9 \text{ MPa}\sqrt{\text{m}}$ , and are labeled A and B in Figure 9, respectively. These fully closed conditions coincide with analytical results for  $t = 360 \text{ \AA}$  and  $700 \text{ \AA}$ , respectively, which are in the expected thickness range, *i.e.* on the order of, but less than,  $1000 \text{ \AA}$ .

<sup>††</sup> Global closure determinations are believed to be especially sensitive to crack closure away from the crack tip. To overcome this potential problem, excess crack wake was removed with a saw blade. Although global and local measurements are in good agreement here, this may not occur if load history effects are important.

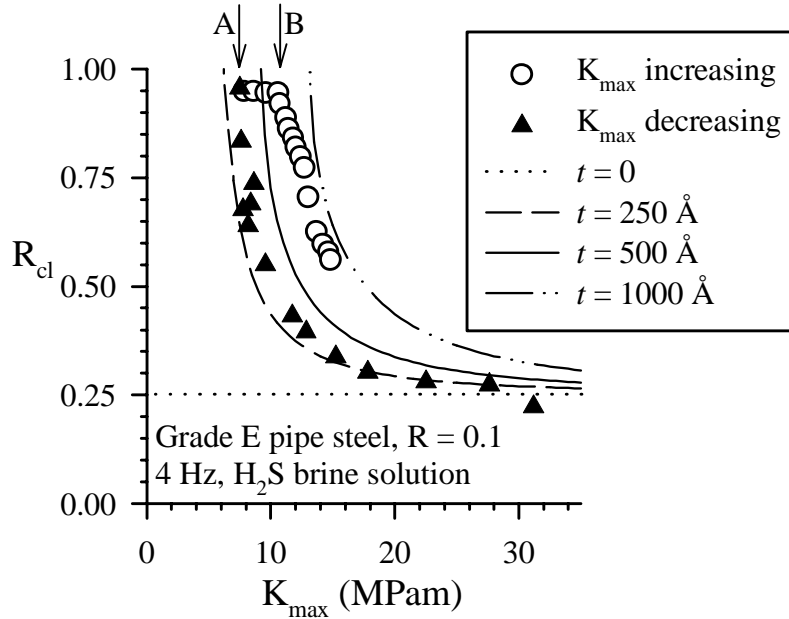


Figure 9. Comparison of model results (solid curve) and experimental data (symbols) published by Ruppen, *et al.* Here only PICC and OICC are considered. Model results are shown for four values of oxide thickness. Model results were found to be in good agreement with experimental data although a specific value of oxide thickness is difficult to determine.

Gray, *et al.* (ref. 19) and Drury, *et al.* (ref. 21) studied RICC effects using fine-grain (FG) and course-grain (CG) heat treatments AISI 1080 steel and Inconel 718 (a nickel-based alloy), respectively. Changes in grain size greatly affects crack roughness, while only slightly changing the yield stress. Therefore, differences in closure behavior between FG and CG versions of these alloys were attributed to RICC. The data of Gray (AISI 1080 steel) and Drury (Inconel 718) are plotted as  $R_{cl}$  against  $K_{max}$  in Figures 10a and 10b, respectively.

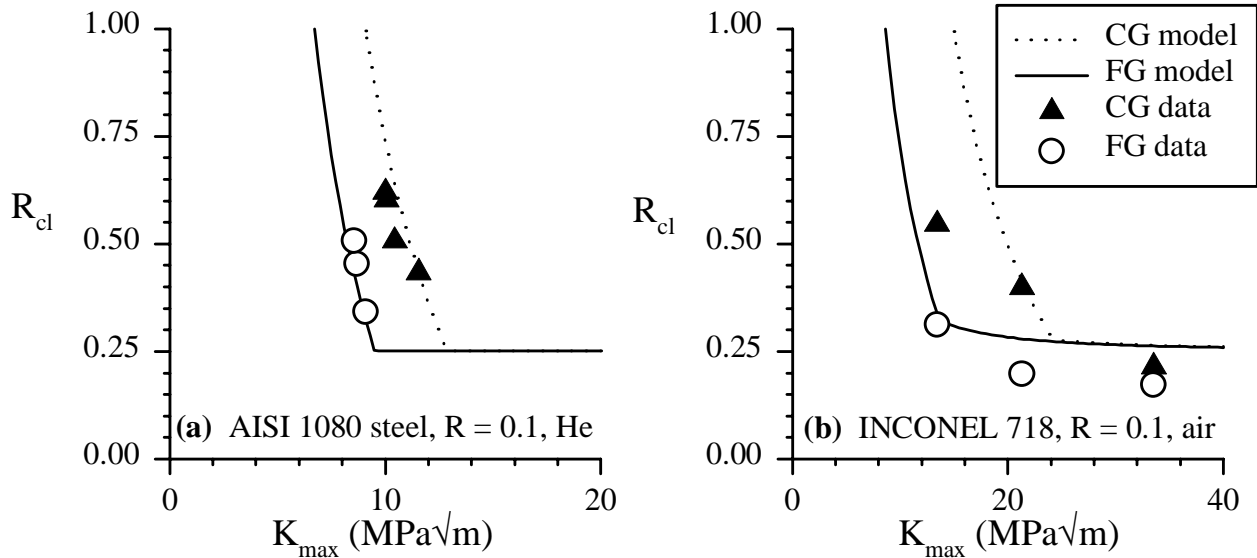


Figure 10. Two plots are shown comparing model results (curve) and experimental data (symbols) for course- and fine-grained alloys. These data were published by (a) Gray, *et al.* and (b) Drury, *et al.*

FG and CG data are shown as open circular and closed triangular symbols, and analytical results for FG and CG configurations are shown as solid and dashed curves, respectively. In Figure 10a, analytical results are in good agreement with the AISI 1080 data. The Inconel 718 data in Figure 10b are also in good agreement with analytical results, with one exception; the CG data point about  $K_{\max} = 12 \text{ MPa}\sqrt{\text{m}}$ . Analytical results indicate the crack-tip is fully closed for this data point, so this closure measurement is likely based on closure events away from the crack-tip instead of crack-tip events. However, changes in model parameters (*e.g.*  $\alpha$ ,  $t$ ,  $g$ , *etc.*) could be made to better fit the experimental results. Selecting model parameters based on experimental data was avoided because empirical relations are likely application specific and not likely to produce any new understanding of closure behavior. The ability to predict general trends in data was considered more important than refining model predictions for specific cases.

## Closure Mechanism Interactions

Analytical results indicate the linear superposition of Equation 1 is not valid and interactions between PICC, RICC, and OICC are non-linear. As an example, consider 2024 aluminum loaded at  $K_{\max} = 3.5 \text{ MPa}\sqrt{\text{m}}$  and  $R = 0.05$  with an oxide layer  $500 \text{ \AA}$  thick. Here PICC, RICC, and OICC are all contributing closure mechanisms and analytical results indicate asperity contact occurs at  $R_{\text{cl}} = 0.713$ . Assuming for now that superposition is valid, this result is expressed symbolically as Equation 2.

$$R_{\text{cl}} = R_{\text{cl}}|_{\text{PICC}} + R_{\text{cl}}|_{\text{RICC}} + R_{\text{cl}}|_{\text{OICC}} = \mathbf{0.713} \quad (2)$$

Contributions from individual closure mechanisms are determined by altering model parameters. The OICC and RICC contributions can be eliminated by setting  $t = 0$  and  $\alpha = 0$ , respectively, to isolate the PICC contribution. Although tip contact would occur for this crack configuration, closure will only be considered  $10 \text{ }\mu\text{m}$  behind the crack tip for consistency (where asperity contact occurred for the result of Equation 2). Analytical results indicate closure occurs at  $R_{\text{cl}} = 0.066$  for this case. PICC is the only closure mechanism, so Equation 1 reduces to Equation 3.

$$R_{\text{cl}}|_{\text{PICC}} = \mathbf{0.066} \quad (3)$$

To consider PICC and OICC, but eliminate RICC, only  $\alpha$  was set to zero. As before, closure is considered  $10 \text{ }\mu\text{m}$  behind the crack tip for consistency. Analytical results predict  $R_{\text{cl}} = 0.363$  for this case, and using superposition, the OICC closure contribution is determined in Equation 4 by substituting Equation 3 into Equation 1.

$$R_{\text{cl}}|_{\text{OICC}} = R_{\text{cl}} - R_{\text{cl}}|_{\text{PICC}} = 0.363 - 0.066 = \mathbf{0.297} \quad (4)$$

PICC and RICC are considered in the absence of OICC by setting  $t = 0$ . Analytical results indicate closure (asperity contact) occurs at  $R_{\text{cl}} = 0.303$  for this case, and the RICC contribution is determined in Equation 5 using the PICC contribution of Equation 3.

$$R_{\text{cl}}|_{\text{RICC}} = R_{\text{cl}} - R_{\text{cl}}|_{\text{PICC}} = 0.303 - 0.066 = \mathbf{0.237} \quad (5)$$

If superposition is valid, the sum of bold terms in Equations 3-5 (0.066, 0.297, and 0.237) will equal the bold term of Equation 2 (0.713). However, the sum of individual contributions is less than the total amount of closure, as shown in Equation 6. Therefore, the linear superposition of Equation 1 is not valid because of non-linear interactions between closure mechanisms.

$$R_{cl} = 0.066 + 0.297 + 0.237 = \mathbf{0.600} < \mathbf{0.713} \quad (6)$$

## Discussion of Results

Analytical results were compared with experimental data in the previous section to validate the CROP closure model. Experiments were conducted to study the influence of each closure mechanism (PICC, RICC, and OICC). Simple crack configurations were considered and satisfied before increasingly complex cases, to allow portions of the model to be validated individually. Additionally, analytical results were compared with data presented in the literature for aluminum, steel, and nickel-based alloys. For all cases considered, analytical results were found in good agreement with experimental data.

For rough cracks, closure is most likely to first occur at the crack-tip or the asperity nearest the crack tip (called tip contact and asperity contact, respectively) depending on loading conditions and geometry. Where PICC is the only closure mechanism (straight crack with no oxide layer), tip contact occurs and closure levels only depend on  $R$  (see Figure 2). Changes in  $R_{cl}$  during constant- $R$  threshold testing are attributed to other closure mechanisms; likely RICC and/or OICC; or load history effects. Closure contributions of RICC and OICC tend to increase as  $K_{max}$  decreases, *i.e.* near threshold, so increased roughness and oxide contributions are expected at threshold (see Figures 3, 4, and 8-10). Where crack roughness is a factor, asperity contact is possible, most likely occurring at lower  $K_{max}$ , lower yield stress ( $\sigma_o$ ), and higher asperity angles ( $\alpha$ ). Analytical results indicate a transition from tip contact to asperity contact occurs during constant- $R$  threshold testing. Further reduction in  $K_{max}$  results in a rapid increase in  $R_{cl}$ , and eventually the crack becomes completely closed (see Figures 8 and 10). However, results shown in Figure 6 indicate thick oxide layers increase the closure levels at the crack tip, reducing the effects of crack roughness.

Both analytical and experimental results indicate crack closure may occur at either the crack tip or its nearest asperity. Local closure determinations were used to show that higher closure levels occurred at the crack tip or its nearest asperity where tip contact or asperity contact was predicted, respectively (refs. 3 and 29). However, the corresponding global data were unable to detect either tip contact or asperity contact. Global closure determinations appear more sensitive to closure events away from the crack tip because the agreement between local and global data improved with increasing distance behind the crack tip. If near-tip closure events are difficult to detect, it might not be possible to determine the actual value of  $\Delta K_{eff}$  with remote compliance data in all cases. Such difficulties in measuring near-tip closure loads may be the reason crack closure does not explain all FCG load ratio effects at threshold. Asperity contact is likely limited to long cracks with a significant rough wake, so accelerated growth of short cracks may be due to the absence of asperity contact (typical of long cracks) and the inability to detect the difference. Further research is needed to determine if threshold load ratio effects and short-crack behavior can be explained in terms of near-tip closure events.

## Summary

In part I of this paper, the CROP closure model was developed that included contributions from, and interactions between, plasticity-, roughness, and oxide-induced crack closure mechanisms (PICC, RICC, and OICC, respectively). This model is uniquely suited to threshold applications because PICC, RICC, and OICC are the closure mechanisms most likely at FCG threshold, but no other model includes all three mechanisms simultaneously. In this paper, the CROP model was shown to be in good agreement with experimental data over a wide range of crack-tip loading (*i.e.* both at threshold and in the Paris regime) and for several different types of alloys (*i.e.* aluminum, steel, nickel-based alloys). From this study a

better understanding of near-threshold crack closure has been achieved, including the following key findings:

- Crack closure is most likely at the crack tip or the asperity nearest the crack tip (called tip contact and asperity contact, respectively).
- Where PICC is the only closure mechanism, closure levels only depend on R.
- A transition to asperity contact occurs as  $K_{\max}$  decreases (for constant-R testing). Further reduction in  $K_{\max}$  results in a rapid increase in closure.
- Crack closure mechanisms interact in a non-linear manner and can only be predicted with a multiple-mechanism model (such as the CROP model).

## References

1. W. Elber, "Fatigue Crack Closure Under Cyclic Tension," *Engineering Fracture Mechanics*, Volume 2, 1970, pp. 37-45.
2. J. A. Newman, W. T. Riddell, and R. S. Piascik, "Modeling the Interactions Between Multiple Crack Closure Mechanisms at Threshold," 2003, NASA-TM-2003-212402.
3. J. A. Newman, "The Effects of Load Ratio on Threshold Fatigue Crack Growth of Aluminum Alloys," Ph.D. dissertation, 2000, Virginia Polytechnic Institute and State University. Available online at: <http://scholar.lib.vt.edu/theses/available/etd-11012000-15010038/>.
4. S. Suresh and R. O. Ritchie, "A Geometric Model for Fatigue Crack Closure Induced by Fracture Surface Roughness," *Metallurgical Transactions*, Volume 13A, 1982, pp. 1627-1631.
5. S. H. Wang, C. Muller, and H. E. Exner, "A Model for Roughness-Induced Fatigue Crack Closure," *Metallurgical and Materials Transactions*, Volume 29A, 1998, pp. 1933-1939.
6. S. Suresh and R. O. Ritchie, "Some Considerations on the Modeling of Oxide-Induced Fatigue Crack Closure Using Solutions for a Rigid Wedge Inside a Linear Elastic Crack," *Scripta Metallurgica*, Volume 17, 1983, pp. 575-580.
7. J. C. Newman, Jr., "FASTRAN II – A Fatigue Crack Growth Structural Analysis Program," 1992, NASA TM-104159.
8. J. Llorca, "Roughness Induced Fatigue Crack Closure: A Numerical Study," *Fatigue and Fracture of Engineering Materials and Structures*, Volume 15, 1992, pp. 665-669.
9. A. M. Garcia and H. Seheitoglu, "Contact of Crack Surfaces During Fatigue: Part 1 – Formulation of the Model," *Metallurgical Transactions*, Volume 28A, 1997, pp. 2263-2275.
10. H. Seheitoglu and A. M. Garcia, "Contact of Crack Surfaces During Fatigue: Part 2 – Simulations," *Metallurgical Transactions*, Volume 28A, 1997, pp. 2277-2289.
11. N. Chen and F. V. Lawrence, "An Analytical Model for Studying Roughness Induced Crack Closure," *Fatigue and Fracture Mechanics*, 29<sup>th</sup> Volume, ASTM STP 1321, T. L. Panontin and S. D. Sheppard, Editors, American Society for Testing and Materials, 1999, West Conshohocken, PA, pp. 535-550.

12. K. S. Ravichandran, "A Theoretical Model for Roughness Induced Crack Closure," *International Journal of Fracture*, Volume 44, 1990, pp. 97-110.
13. K. S. Ravichandran, "Further Results on 'A Theoretical Model for Roughness Induced Crack Closure'; Effect of Yield Strength and Grain Size," *International Journal of Fracture*, Volume 44, 1990, pp. R23-R26.
14. W. T. Riddell and R. S. Piascik, M. A. Sutton, W. Zhao, S. R. McNeill, and J. D. Helm, "Determining Fatigue Crack Opening Loads from Near-crack-tip Displacement Measurements," *Advances in Fatigue Crack Closure Measurement and Analysis 2<sup>nd</sup> Vol. ASTM STP 1343*, American Society for Testing and Materials, West Conshohocken, PA, 1999, pp. 157-174.
15. P. C. Paris, H. Tada, and J. K. Donald, "Service Load Fatigue Damage – A Historical Perspective." *Proceedings of Fatigue Damage of Structural Materials II*, 1998, Cape Cod, MA, Sept. 7-11.
16. J. C. Newman, Jr., "Analyses of Fatigue Crack growth and Closure Near Threshold Conditions for Long-Crack Behavior," *Fatigue Crack Growth Thresholds, Endurance Limits, and Design, ASTM STP 1372*, J. C. Newman, Jr. and R. S. Piascik, Editors, American Society for Testing and Materials, 2000, West Conshohocken, PA, pp. 227-251.
17. R. C. McClung, "Analyses of Fatigue Crack Closure During Simulated Threshold Testing," *Fatigue Crack Growth Thresholds, Endurance Limits and Design. ASTM STP 1372*, J. C. Newman, Jr. and R. S. Piascik, Editors, American Society for Testing and Materials, 2000, West Conshohocken, PA, pp. 209-226.
18. A. J. McEvily, "Fatigue Fracture-Surface Roughness and the K-Opening Level," *International Journal of Fatigue*, Volume 19, 1997, pp. 629-633.
19. G. T. Gray III, J. C. Williams, and A. W. Thompson, "Roughness Induced Crack Closure: An Explanation for Microstructurally Sensitive Fatigue Crack Growth," *Metallurgical Transactions*, Volume 14A, 1983, pp. 421-433.
20. J. A. Ruppen and R. Salzbrenner, "The Effect of Environment on Crack Closure and Fatigue Threshold," *Fatigue of Engineering Materials and Structures*, Volume 6, 1983, pp. 307-314.
21. W. J. Drury, A. M. Gokhale, and S. D. Antolovich, "Effect of Crack Surface Geometry on Fatigue Crack Closure," *Metallurgical and Materials Transactions*, Volume 26A, 1995, pp. 2651-2663.
22. W. F. Deans, C. B. Jolly, W. A. Poyton, and W. Watson, "A Strain Gauging Technique for Monitoring Fracture Mechanics Specimens During Environmental Testing," *Strain*, Volume 13, 1977, pp. 152-154.
23. ASTM Standard E647, *Standard Test Method for Measurement of Fatigue Crack Growth Rates*, Annual Book of ASTM standards, Volume 3.01, American Society for Testing and Materials, 2001, West Conshohocken, PA.
24. R. S. Piascik, J. C. Newman, Jr., and J. H. Underwood, "The Extended Compact Tension Specimen," *Fatigue and Fracture of Engineering Materials and Structures*, Volume 20, 1997, pp. 559-563.
25. W. Elber, "Crack Closure and Crack Growth Measurements in Surface-Flawed Titanium Alloy Ti-6Al-4V," 1975, NASA TN-D-8010.
26. S. W. Smith and R. S. Piascik, "An Indirect Technique for Determining Closure-Free Fatigue Crack Growth Behavior," *Fatigue Crack Growth Thresholds, Endurance Limits and Design, ASTM STP 1372*, J. C. Newman, Jr. and R. S. Piascik, Editors, American Society for Testing and Materials, 2000, West Conshohocken, PA, pp. 109-122.

27. M. A. Sutton, Y. J. Chao, and J. S. Lyons, "Computer Vision Methods for Surface Deformation Measurements in Fracture Mechanics," *Novel Experimental Techniques in Fracture Mechanics*, AMD-Volume 176, American Society for Mechanical Engineers, 1993, pp. 203-217.
28. M. A. Sutton, W. Zhao, S. R. McNeill, J. D. Helm, R. S. Piascik, and W. T. Riddell, "Local Crack Closure Measurements: Development of a Measurement System Using Computer Vision and a Far Field Microscope," *Second Symposium on Crack Closure Measurement and Analysis, ASTM STP 1343*, R. C. McClung and J. C. Newman, Jr., Editors, American Society for Testing and Materials, West Conshohocken, PA.
29. J. A. Newman and R. S. Piascik, "Plasticity and Roughness Closure Interactions at Threshold," *Fatigue and Fracture Mechanics: 33<sup>rd</sup> Volume, ASTM STP 1417*, W. G. Rueter and R. S. Piascik, Editors, American Society for Testing and Materials, 2002, West Conshohocken, PA.
30. A. P. Reynolds, "Constant Amplitude and Post-Overload Fatigue Crack Growth Behavior in PM Aluminum Alloy AA 8009," *Fatigue and Fracture of Engineering Materials and Structures*, Volume 15, 1992, pp. 551-562.
31. M. S. Hunter and P. Fowle, "Natural and Thermally Formed Oxide Films on Aluminum," *Journal of the Electrochemical Society*, Volume 103, 1956, pp. 482-485.

REPORT DOCUMENTATION PAGE			Form Approved OMB No. 0704-0188	
Public reporting burden for this collection of information is estimated to average 1 hour per response, including the time for reviewing instructions, searching existing data sources, gathering and maintaining the data needed, and completing and reviewing the collection of information. Send comments regarding this burden estimate or any other aspect of this collection of information, including suggestions for reducing this burden, to Washington Headquarters Services, Directorate for Information Operations and Reports, 1215 Jefferson Davis Highway, Suite 1204, Arlington, VA 22202-4302, and to the Office of Management and Budget, Paperwork Reduction Project (0704-0188), Washington, DC 20503.				
1. AGENCY USE ONLY (Leave blank)		2. REPORT DATE May 2003	3. REPORT TYPE AND DATES COVERED Technical Memorandum	
4. TITLE AND SUBTITLE Analytical and Experimental Study of Near-Threshold Interactions Between Crack Closure Mechanisms			5. FUNDING NUMBERS 706-61-11-03	
6. AUTHOR(S) John A. Newman, William T. Riddell, and Robert S. Piascik				
7. PERFORMING ORGANIZATION NAME(S) AND ADDRESS(ES) NASA Langley Research Center Hampton, VA 23681-2199			8. PERFORMING ORGANIZATION REPORT NUMBER L-18207	
9. SPONSORING/MONITORING AGENCY NAME(S) AND ADDRESS(ES) National Aeronautics and Space Administration Washington, DC 20546-0001 and U.S. Army Research Laboratory Adelphi, MD 20783-1145			10. SPONSORING/MONITORING AGENCY REPORT NUMBER NASA/TM-2003-211755 ARL-TR-2774	
11. SUPPLEMENTARY NOTES				
12a. DISTRIBUTION/AVAILABILITY STATEMENT Unclassified-Unlimited Subject Category 26                      Distribution: Standard Availability: NASA CASI (301) 621-0390			12b. DISTRIBUTION CODE	
13. ABSTRACT (Maximum 200 words) The results of an analytical closure model – that considers contributions and interactions between plasticity-, roughness-, and oxide-induced crack closure mechanisms – are presented and compared with experimental data. The analytical model is shown to provide a good description of the combined influences of crack roughness, oxide debris, and plasticity in the near-threshold regime. Furthermore, analytical results indicate that closure mechanisms interact in a non-linear manner such that the total amount of closure is not the sum of closure contributions for each mechanism.				
14. SUBJECT TERMS Fatigue crack growth, Crack closure, Plasticity, Roughness, Oxide, Crack tip, Experiment, Threshold			15. NUMBER OF PAGES 21	
			16. PRICE CODE	
17. SECURITY CLASSIFICATION OF REPORT Unclassified	18. SECURITY CLASSIFICATION OF THIS PAGE Unclassified	19. SECURITY CLASSIFICATION OF ABSTRACT Unclassified	20. LIMITATION OF ABSTRACT UL	